Journal of Molecular Spectroscopy 373 (2020) 111373

Contents lists available at ScienceDirect

Journal of Molecular Spectroscopy

journal homepage: www.elsevier.com/locate/jms

An analysis of the rotational ground state and lowest-energy vibrationally excited dyad of 3-cyanopyridine: Low symmetry reveals rich complexity of perturbations, couplings, and interstate transitions

P. Matisha Dorman, Brian J. Esselman, R. Claude Woods *, Robert J. McMahon *

Department of Chemistry, University of Wisconsin–Madison, Madison, WI 53706, USA

ARTICLE INFO

Article history:
Received 25 May 2020
In revised form 22 August 2020
Accepted 3 September 2020
Available online 11 September 2020

Keywords:
Cyanopyridine
Millimeter-wave
Rotational spectroscopy
Excited vibrational states
Coriolis coupling
Astrochemistry

ABSTRACT

The rotational spectrum of 3-cyanopyridine from 130 to 360 GHz was recorded, and an analysis of the ground state and two lowest-energy excited vibrational states was completed. Almost 6700 new transitions were measured for the ground state and fit to a partial octic, distorted-rotor Hamiltonian with low error (σ_{fit} < 0.05 MHz). The first two excited vibrational states, ν_{30} and ν_{21}, are an isolated dyad that exhibits both *a*- and *b*-type Coriolis perturbations and requires a two-state, least-squares fit to fully predict the rotational spectrum and determine accurate spectroscopic constants. Quartic and sextic distortion constants were determined for the dyad, along with seven symmetry-allowed perturbation terms: $G_a, G_a^J, F_{bc}, F_{bc}^K, G_b, G_b^J$, and G_b^K. Numerous resonances, including those following *a*-type selection rules, ΔK_a = 2 or ΔK_a = 4, and *b*-type selection rules, ΔK_a = 3 or ΔK_a = 5, were observed and fit. For ν_{30} and ν_{21}, the energy difference ($\Delta E_{30,21}$ = 15.7524693 (37) cm^{-1}), both Coriolis coupling constants ($\zeta^a_{30,21}$ = 0.8327 (9) and $\zeta^b_{30,21}$ = −0.0181 (3)), and vibration–rotation interaction constants were determined experimentally and compared to theoretical values determined computationally. Combined with the work on the vibrationally excited dyads of 4-cyanopyridine, phenyl isocyanide, benzonitrile, and phenylacetylene, the coupling in ν_{30} and ν_{21} provides an opportunity to compare the Coriolis interactions of these analogous mono-substituted aromatic molecules in unusual detail. Additionally, this work improves the ground-state rotational constants and centrifugal distortion constants of 3-cyanopyridine and provides the fundamental constants needed to support an astronomical search for 3-cyanopyridine in the interstellar medium.

1. Introduction

Obtaining direct evidence of nitrogen-containing aromatic rings in the interstellar medium (ISM) is a significant objective in astrochemistry and motivates our research on the cyanopyridine isomers [1]. The 2-, 3-, and 4-cyanopyridines (Fig. 1) are molecules of particular interest to astrochemistry due to their large dipole moments (μ = 5.78, 3.66, and 1.96 D, respectively) [2], heteroatom-containing aromatic ring, and similarity to benzonitrile. Nitriles have been detected in the ISM [3] and are abundant in the atmosphere of Saturn's largest moon, Titan [4]. The recent detection of the substituted aromatic molecule, benzonitrile (C_6H_5CN), in Taurus Molecular Cloud 1 [5] stimulated the consideration of other possible precursors of nitrogenous polycyclic aromatic organic molecules that may exist in the ISM.

3-Cyanopyridine is a C_s, near-prolate (κ = −0.854), asymmetric rotor with experimentally measured dipole moment components of 3.13 D along the *a*-inertial axis and 1.90 D along the *b*-inertial axis [2]. These large dipole moment components for a molecule of this mass distribution give rise to a dense spectrum of *a*- and *b*-type absorptions that include both R- and Q-branch transitions in our observed frequency range. Of the cyanopyridine isomers, 3-cyanopyridine (Fig. 2) is the least investigated by rotational spectroscopy. Ford experimentally determined the rotational constants and dipole moments of all the cyanopyridine isomers and reported twenty-two microwave transitions from 8 to 24 GHz for 3-cyanopyridine [2]. The energies of the vibrational modes, including ν_{30} (A'', 160 cm^{-1}) and ν_{21} (A', 176 cm^{-1}), have been determined *via* solid-state Raman spectroscopy [6,7]. Recently, Khaikin *et al.* [8,9] determined an equilibrium structure of 3-cyanopyridine using a combination of data from newly recorded gas-phase electron diffraction and previously published microwave studies.

* Corresponding author.
E-mail addresses: rcwoods@wisc.edu (R.C. Woods), robert.mcmahon@wisc.edu (R.J. McMahon).

https://doi.org/10.1016/j.jms.2020.111373
0022-2852/

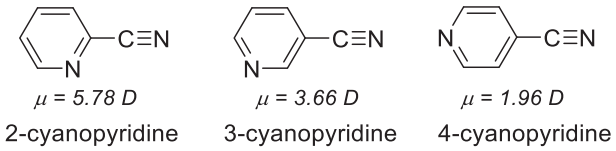

Fig. 1. Cyanopyridine isomers with experimental dipole moments.

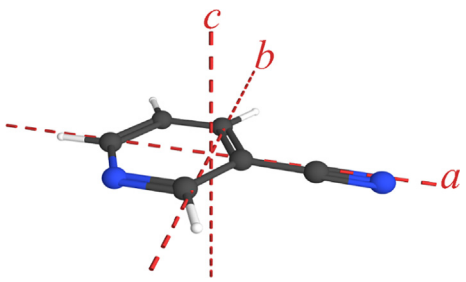

Fig. 2. 3-Cyanopyridine structure with principal inertial axes (μ_a = 3.13 D and μ_b = 1.90 D).

In the current study, the rotational spectrum of the ground vibrational state of 3-cyanopyridine (including 6701 independent transitions) was fit to a partial octic, single-state distorted-rotor Hamiltonian. The two lowest-lying excited vibrational states, ν_{30} and ν_{21}, are close enough in energy that their rotational levels cross, causing local and global frequency perturbations to their rotational spectra. The data for these two states, which include 7134 independent transitions, were fit using a two-state model. Quartic and sextic distortion constants, along with seven Coriolis perturbation terms and a very precise value of the energy difference between the states, were determined. This treatment addresses both *a*- and *b*-type resonances and permits the measurement of several *b*-type, Coriolis-allowed nominal interstate transitions.

Our earlier studies provided significant insights into the fundamental chemical physics, the quantum mechanical state-mixing phenomena, and the spectroscopic consequences for prototypical mono-substituted aromatic molecules (4-cyanopyridine [1], phenyl isocyanide [10], benzonitrile [11]). The previously studied molecules, however, were each of C_{2v} symmetry and thus exhibited only *a*-type rotational transitions. By virtue of its lower symmetry (C_s), 3-cyanopyridine exhibits a much richer palette of spectroscopic features: *a*- and *b*-type rotational transitions, *a*- and *b*-type Coriolis couplings, and two matched pairs of *b*-type nominal interstate transitions. The analysis of these features reveals new insights concerning quantum interferences between the Coriolis couplings in these manifolds and raises new questions about the factors governing the strength of Coriolis couplings and the intensity of nominal interstate transitions.

2. Experimental methods

3-Cyanopyridine was purchased commercially (Aldrich, 98% purity) and used without further purification. Using a millimeter-wave spectrometer that has been previously described [10,12,13], the rotational spectrum of 3-cyanopyridine was collected from 130–230 and 235–360 GHz in a continuous flow with a sample pressure of 5–10 mTorr at room temperature. The separate spectral segments were combined into a single broadband spectrum using Kisiel's Assignment and Analysis of Broadband Spectra (AABS) software [14,15]. Pickett's SPFIT/SPCAT [16] was used for least-squares fits and spectral predictions, along with the PIFORM, PMIXC, PLANM, and AC programs for analysis [17]. An uncertainty of 0.050 MHz was assumed for all measurements in the current study, and an uncertainty of 0.080 MHz was assumed for the measured transitions reported in the literature, whose measurement uncertainty was not given.

3. Computational methods

Computations were performed at the B3LYP/6-311+G(2d,p) level of theory using Gaussian 16 program [18] through the WebMO interface [19]. An optimized geometry of 3-cyanopyridine was obtained using "very-tight" convergence criteria with an "ultrafine" integration grid. Vibration-rotation interaction constants, quartic and sextic centrifugal distortion constants, fundamental vibrational frequencies, and Coriolis coupling constants (ζ) were predicted from an anharmonic vibrational frequency calculation. All computational output files are provided in the supplementary material.

4. Analysis of rotational spectra

4.1. Ground state

3-Cyanopyridine has a substantial dipole moment along both its *a*- and *b*-inertial axes (μ_a = 3.13 D, μ_b = 1.90 D) [2], resulting in a ground-state rotational spectrum composed of quadruply degenerate (in K_c) *a*- and *b*-type transitions at low values of K_a. These quadruply degenerate transitions lose degeneracy as K_a increases, eventually becoming degenerate in K_a with other transitions. 3-Cyanopyridine has a band structure very similar to previously investigated mono-substituted aromatic molecules 4-cyanopyridine [1], phenyl isocyanide [10], benzonitrile [11], and phenylacetylene [20], except with the addition of many *b*-type R-branch transitions. Almost 6700 new independent transitions were measured in the 130–360 GHz region (σ_{fit} = 0.043 MHz), including *a*- and *b*-type R-branch transitions with K_a values ranging from 0 to 63 and J'' values from 46 to 118. Weak *a*- and *b*-type Q-branch series, with K_a values ranging from 2 to 35 and J'' values from 20 to 127, were assigned and fit with low error. A portion of the experimental spectrum in the 199–200 GHz region is provided in Fig. 3, which highlights the ground vibrational state and the two lowest-lying fundamentals, ν_{30} and ν_{21}.

The data distribution plot in Fig. 4 displays the large number of newly measured rotational transitions, along with the 10–24 GHz microwave transitions [2]. The size of the circles is represented by $|(f_{obs.} - f_{calc.})/\delta f|$, where δf is the measurement uncertainty (0.050 MHz). At high frequency, a large number of transitions from other vibrational states and harmonics tend to complicate the spectrum, leading to an increase in the error and size of the distribution plot circles at high J''. (This increase is also partially due to the simple fact that higher J transitions occur at higher frequencies, which naturally are prone to having higher errors relative to a δf value assumed to be fixed.) Addition of higher-order centrifugal distortion parameters to the least-squares fit did not change this trend or improve the overall error.

The rotational spectrum of 3-cyanopyridine was fit to a partial octic, distorted-rotor Hamiltonian in the A-reduced, I^r representation (Table 1), a choice supported by a desire to be consistent with previously published work on this series of molecules. Initial spectral predictions were made using experimentally determined rotational constants from Ford's work [2] and computationally predicted quartic centrifugal distortion constants. All quartic and sextic distortion constants were determined for the first time for 3-cyanopyridine, as were three of the on-diagonal octic distortion terms, L_{JJK}, L_{JK}, and L_{KKJ}. The computed centrifugal distortion constants (except Δ_K and Φ_J) agree to within 8% and 16% of the

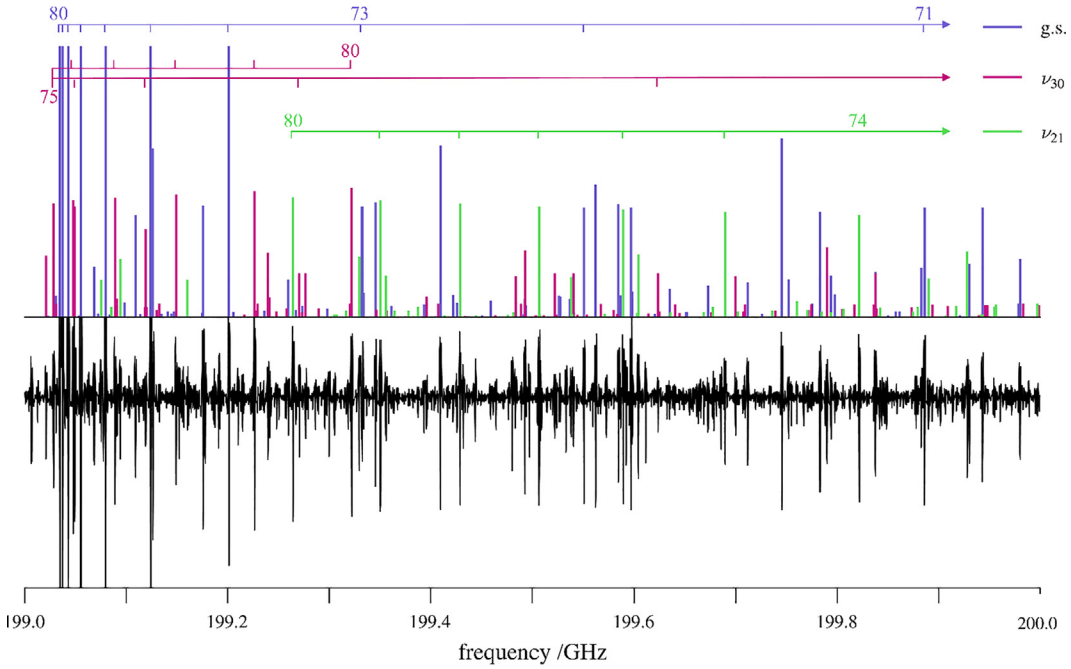

Fig. 3. Experimental rotational spectrum (bottom) of 3-cyanopyridine from 199.0 to 200.0 GHz and predicted stick spectra (top). The ground state (purple), ν_{30} (pink), and ν_{21} (green) are labeled by the upper state quantum number J'' + 1.

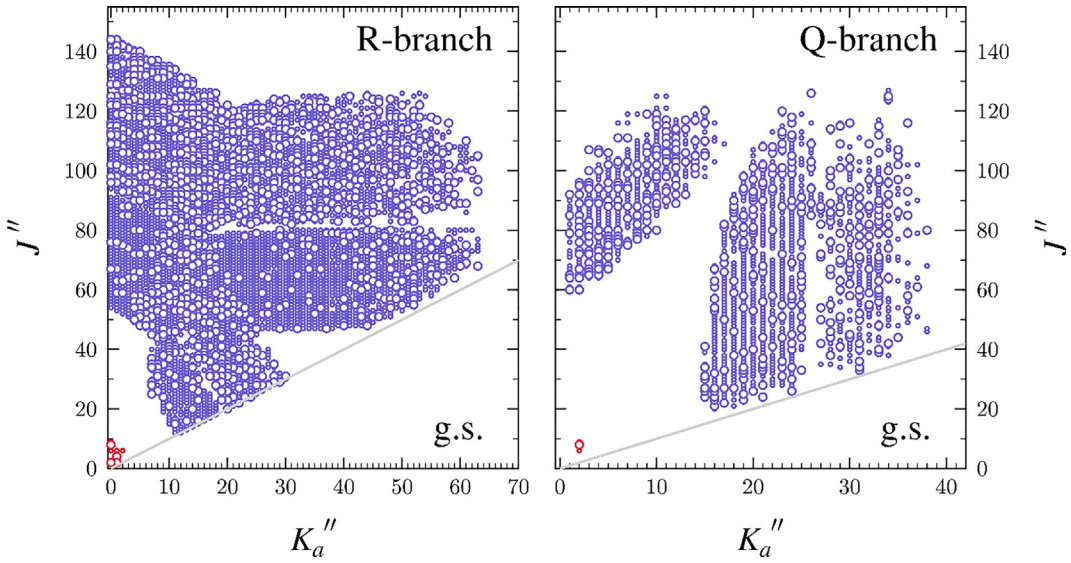

Fig. 4. Data distribution plots for the least-squares fit of spectroscopic data for the vibrational ground state of 3-cyanopyridine (A-reduction, I^r representation). The size of the outlined circles in this plot corresponds to $|(f_{obs.} - f_{calc.})/\delta f|$, where δf is the measurement uncertainty. Purple symbols denote data from the present work, red symbols denote data from Ford.[2]

experimental distortion constants for the quartic and sextic terms, respectively. All computed constants were smaller than their experimental counterparts except Δ_K. Given the quality of the least-squares fit of the experimental data, the discrepancy in Δ_K appears to lie in its computed value. This situation is similar to DFT treatments of analogous species (see discussion). In the case of Φ_J, the origin of the large difference between the computed and experimental values is more ambiguous and warrants careful consideration. Some of the sextic and octic centrifugal distortion constants, such as Φ_J and L_{JJK}, are difficult to determine, even with greater than 6000 transitions in the final least-squares fit. To investigate the inclusion of Φ_J in the least-squares fitting, a new fit was obtained in which Φ_J was held constant at its computed value. Constraining Φ_J to its computed value did not significantly alter or improve the determination of the other spectroscopic constants but did slightly increase the σ_{fit} value. Thus, Φ_J was allowed to vary in the final least-squares fit presented in Table 1. Due to the lack of computed octic centrifugal distortion constants in any readily available computational software package, each term was independently investigated in a similar manner to determine which octic terms should be included in the fit or held constant at zero. Least-squares fitting files of the A-reduced ground-state fit of 3-cyanopyridine are included in the supplementary material.

Table 1
Spectroscopic constants for the ground vibrational state of 3-cyanopyridine (A-reduced Hamiltonian, I^r representation).

	Ford [2]	Current work[a]	B3LYP[b]	% difference
$A_0^{(A)}$ (MHz)	5823.01 (5)	5823.05832 (11)	5826.3	−0.1
$B_0^{(A)}$ (MHz)	1571.34 (3)	1571.351896 (30)	1570.4	0.1
$C_0^{(A)}$ (MHz)	1237.17 (3)	1237.169980 (23)	1237.7	0.0
Δ_J (kHz)		0.0464884 (30)	0.0446	4.1
Δ_{JK} (kHz)		1.063742 (28)	0.993	6.7
Δ_K (kHz)		0.23366 (16)	0.281	−20.3
δ_J (kHz)		0.0110955 (13)	0.0106	4.5
δ_K (kHz)		0.673712 (34)	0.626	7.1
Φ_J (Hz)		0.00000360 (12)	0.00000229	36.4
Φ_{JK} (Hz)		0.0018504 (47)	0.00157	15.1
Φ_{KJ} (Hz)		−0.009199 (21)	−0.00789	14.2
Φ_K (Hz)		0.007488 (69)	0.00693	7.5
ϕ_J (Hz)		0.000001213 (58)	0.00000106	12.6
ϕ_{JK} (Hz)		0.0009081 (26)	0.000795	12.5
ϕ_K (Hz)		0.009045 (65)	0.00783	13.4
L_{JJK} (μHz)		−0.00242 (10)		
L_{JK} (μHz)		0.01754 (61)		
L_{KKJ} (μHz)		−0.1407 (34)		
N_{lines}[c]	22	6701		
σ_{fit} (MHz)		0.043		
Δ_i (uÅ^2)[d]	0.08 (1)	0.086225 (10)		

[a] Includes transitions from Ford [2].
[b] B3LYP/6-311+G(2d,p) values converted to a right-handed coordinate system.
[c] Number of assigned transition frequencies.
[d] Inertial defect ($\Delta_i = I_c - I_a - I_b$).

4.2. Lowest-energy fundamental vibrational states ν_{30} and ν_{21}

As in the 4-cyanopyridine isomer, the two lowest-energy fundamental vibrational states of 3-cyanopyridine occur approximately 150 cm^{-1} above the ground state and are sufficiently close in energy to allow Coriolis coupling between the rotational energy levels. This interaction results in *a*-type and *b*-type Coriolis coupling that produces both local and global perturbations to the rotational spectrum. In Fig. 5, the vibrational manifold of 3-cyanopyridine is shown up to 500 cm^{-1}. The lower-energy vibration, ν_{30} (A'', 160 cm^{-1}), is an out-of-plane bend of the cyano group with respect to the plane of the pyridine ring, while ν_{21} (A', 176 cm^{-1}) is an in-plane wag of the cyano group. These fundamental modes and relative energies are consistent in all three cyanopyridine isomers, with the out-of-plane mode lying ~10–20 cm^{-1} lower in energy than the in-plane mode. The reduced symmetry in 3-cyanopyridine (C_s), relative to 4-cyanopyridine (C_{2v}), changes the symmetry labeling of the vibrational states and consequently reverses the order of the state numbering. Above the low-energy dyad (ν_{30} and ν_{21}) lies a series of states with complicated Coriolis and Fermi couplings. These states, which are expected to be difficult to analyze and assign, are not addressed in the current study. A table containing experimental [6,7] and computed values of the harmonic and anharmonic vibrational frequencies, associated symmetries, and infrared intensities of each fundamental vibration of 3-cyanopyridine is provided in the supplementary material.

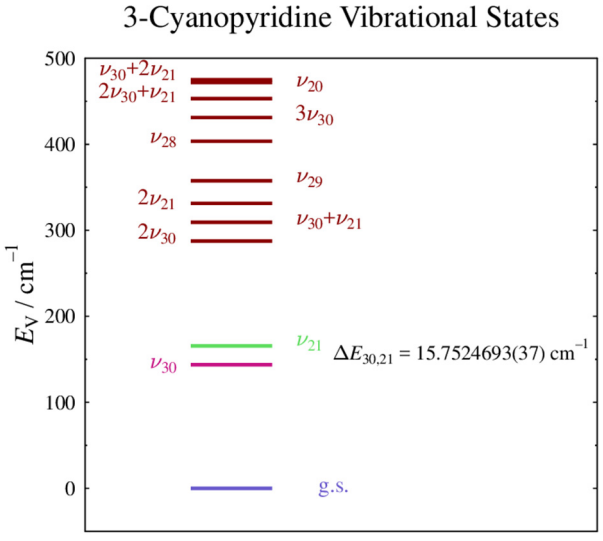

Fig. 5. Vibrational energy levels of 3-cyanopyridine below 500 cm^{-1} from computed fundamental frequencies (B3LYP/6-311+G(2d,p). The value of $\Delta E_{30,21}$ results from the experimental perturbation analysis of ν_{30} and ν_{21} in this work.

Given the structural similarities between 3-cyanopyridine and other systems that we have investigated recently (4-cyanopyridine [1], phenyl isocyanide [10], benzonitrile [11], 2-cyanopyridine [21]), we anticipated that a two-state model would be required to successfully treat the low-lying vibrational states (ν_{30} and ν_{21}) of 3-cyanopyridine. As expected, only K_a = 0, 1, and 2 were able to be successfully fit in a single-state model, even when the distortion constants were allowed to converge to physically meaningless values (inconsistent in sign or order of magnitude with respect to the corresponding ground-state constant). For 3-cyanopyridine (C_s symmetry), both *a*- and *b*-type Coriolis coupling are allowed between ν_{30} (A'') and ν_{21} (A'). In general, a Coriolis-coupling constant ($\zeta^x_{30,21}$) along an arbitrary axis (x) is directly related to the corresponding spectroscopic parameter G_x by equation (1),

$$G_x = \frac{\omega_{30}+\omega_{21}}{\sqrt{\omega_{30}\times\omega_{21}}}\zeta^x_{30,21}B^x_e \approx 2\zeta^x_{30,21}B^x_e \quad (1)$$

where ω_{30} and ω_{21} are the harmonic frequencies for each vibrational state and B^x_e is the equilibrium rotational constant [22]. A two-state treatment was constructed, starting with the experimental ground-state spectroscopic constants, dyad energy difference (ΔE), predicted coupling terms (G_a, G_b), and vibration–rotation interaction constants (α_B, α_C only). Only ΔE, B_v, and C_v were allowed to vary during initial least-squares fitting and, with the inclusion of additional K_a series, additional spectroscopic parameters were allowed to vary, only if they maintained the same sign and similar magnitude as the ground-state value. The fit was iteratively

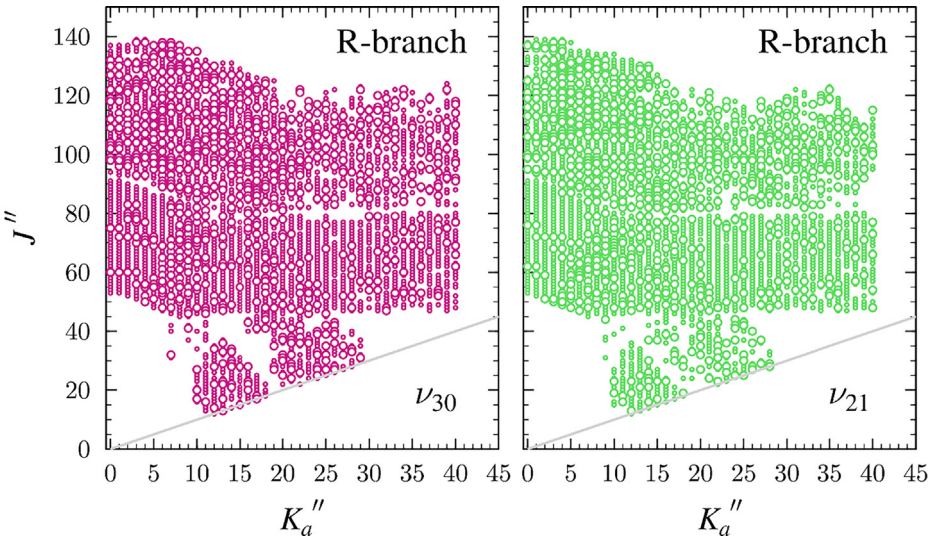

Fig. 6. Data distribution plots for the coupled fit of measured transitions in the two lowest-energy excited vibrational states of 3-cyanopyridine. The size of the outlined circle is proportional to the value of $|(f_{obs.} - f_{calc.})/\delta f|$, where δf is the measurement uncertainty (assumed to be 0.050 MHz).

updated, and the spectrum was re-predicted until all transitions could be fit and resonances modeled adequately.

The excited vibrational states, ν_{30} and ν_{21}, have *a*-type band structures quite similar to those observed for the dyads of 4-cyanopyridine [1], phenyl isocyanide [10], benzonitrile [11], and phenylacetylene [20]. Unfortunately, the predicted Q-branch transitions in these excited vibrational states were too weak to be confidently assigned. For 3-cyanopyridine, a total of 7134 distinct lines were fit for the dyad with J'' values ranging from 12 to 140 and K_a values from 0 to 40. Data distribution plots for ν_{30} and ν_{21} are displayed in Fig. 6. As is observed in the ground-state distribution plot, a similar increase in error at high J'' suggests that any untreated effects apply to both the single-state and dyad least-squares fits.

The spectroscopic parameters determined for the dyad fit of ν_{30} and ν_{21} are displayed in Table 2 and include a precise determination of the energy difference ($\Delta E_{30,21}$) and seven Coriolis-coupling coefficients, $G_a, G_a^J, F_{bc}, F_{bc}^K, G_b, G_b^J$,and G_b^K. Unlike the works on dyads with only *a*-type perturbation [1,10,11,20], the analysis for 3-cyanopyridine required that we fit Δ_K independently for each vibrational state, in order to include high-frequency *b*-type transitions. We were unable, however, to simultaneously determine A_v and Φ_K for each vibrational state. Instead, the least-squares fit varies the average of the *A* rotational constants ($A_+ = \frac{A_{30}+A_{21}}{2}$) and holds constant the half difference ($A_- = \frac{A_{30}-A_{21}}{2}$) at zero. In a similar fashion, the average of Φ_K was determined for the dyad while the half difference was held at zero. The quartic and sextic terms that were allowed to vary all correspond in sign and order of magnitude to the ground-state constants. Least-squares fitting files of the dyad fit of 3-cyanopyridine are included in the supplementary material.

5. Interpretation and analysis of the resonances

The *a*-type resonances display selection rules of ΔK_a = 2 and ΔK_a = 4 between the vibrational states, while the *b*-type resonances display selection rules of ΔK_a = 3 and ΔK_a = 5. Examples of matching pairs of *a*-type resonances (ΔK_a = 2) and *b*-type resonances (ΔK_a = 3) are shown in Fig. 7. The intensity difference between the *a*- and *b*-type resonances can be seen by comparing the scales of the vertical axes in Fig. 7(a) and Fig. 7(b). The ground state is the reference in these plots; both *y*-axes for each mutually perturbing series are presented on the same scale to allow for direct visual comparison. The magnitude of the resonances is evaluated by measuring the largest vertical displacement of the resonance from a frequency predicted in the absence of a local perturbation. For the resonances with small frequency shifts on the hill or valley of an undulation, we can typically estimate the size directly from the resonance plot. Using this simple approach, an approximate magnitude of the ν_{21} resonance (red arrow) depicted in Fig. 7(a) is 0.7 MHz × 79 ≈ 55 MHz. Using a more sophisticated approach, the magnitudes of the resonances were determined using a linear regression method and depicted by dashed arrows in Fig. 7(a) and Fig. 7(b).

The *a*-type resonances begin at $K_a = 0^+$ for ν_{21} and $K_a = 4^-$ for ν_{30}, with small frequency shifts of only a few MHz from the globally perturbed frequency. These resonances progress regularly (approximately every three *J* values) and increase in amplitude with increasing K_a. Toward the high end of our frequency and K_a range, the largest observed *a*-type resonance exhibits a substantial frequency shift of 1078 MHz. The observed *a*-type resonances have even selection rules, which require that the resonances occur between K_a^+ of one state and K_a^- of the other. On the other hand, the observed *b*-type resonances have odd selection rules, which require that the resonances occur between K_a series of the same plus or same minus symmetry. Large ΔK_a = 3, *b*-type resonances appear, starting at the degenerate K_a = 25 for ν_{21} and K_a = 28 for ν_{30}, with frequencies already shifted by hundreds of MHz. The resonances increase in amplitude with increasing K_a until they stop at K_a = 29 for ν_{21} and K_a = 32 for ν_{30}. A plot depicting the progression of these resonances is shown in Fig. 8(a). The first two resonances are separated by a change in *J* of 32, but, with each successive K_a resonance, the change in *J* decreases. The last *b*-type resonance, shown in Fig. 8(a), is separated from the resonance in the prior series by a change in *J* of 11. In Fig. 8(b), a plot of the J'' + 1 values at the most perturbed resonance frequency in each K_a series is fit to a 3rd-order polynomial to high accuracy (R^2 = 0.9996), demonstrating the non-linear progression of the *b*-type resonances, compared to the linear progression of the *a*-type resonances.

Table 2
Spectroscopic constants for the ground vibrational states and coupled dyads of 3-cyanopyridine and 4-cyanopyridine (A-reduced Hamiltonian, I^r representation).

	3-Cyanopyridine			4-Cyanopyridine [1]		
	Ground State	ν_{30} (A'', 160 cm^{-1})[a]	ν_{21} (A', 176 cm^{-1})[a]	Ground State	ν_{20} (B_1, 147 cm^{-1})	ν_{30} (B_2, 166 cm^{-1})
$A_v^{(A)}$ (MHz)	5823.05832 (11)	A_+ (MHz)[b] = 5822.36718 (26)		6000.67028 (91)	A_+ (MHz)[b] = 5999.9708 (19)	
$B_v^{(A)}$ (MHz)	1571.351896 (30)	1573.126189 (50)	1574.409958 (59)	1541.180078 (12)	1542.964930 (63)	1544.087835 (59)
$C_v^{(A)}$ (MHz)	1237.169980 (23)	1239.053308 (47)	1238.071874 (51)	1225.999666 (11)	1227.909675 (65)	1226.885656 (62)
Δ_J (kHz)	0.0464884 (30)	0.0472363 (50)	0.0475523 (56)	0.0469997 (26)	0.0477615 (49)	0.0479672 (52)
Δ_{JK} (kHz)	1.063742 (28)	1.07350 (34)	1.03054 (34)	0.977719 (47)	0.98416 (58)	0.94690 (59)
Δ_K (kHz)	0.23366 (16)	0.24171 (63)	0.26803 (61)	0.3319 (27)	Δ_{K+} (MHz)[b] = 0.3474 (33)	
δ_J (kHz)	0.0110955 (13)	0.0111732 (26)	0.0114978 (30)	0.01103714 (53)	0.0111043 (13)	0.0113867 (12)
δ_K (kHz)	0.673712 (34)	0.67278 (17)	0.67896 (14)	0.64553 (17)	0.64487 (27)	0.65010 (27)
Φ_J (Hz)	0.00000360 (12)	0.00000311 (23)	0.00000528 (26)	0.00000295 (11)	0.00000349 (19)	0.00000442 (20)
Φ_{JK} (Hz)	0.0018504 (47)	0.0016326 (91)	0.0020365 (85)	0.001718 (11)	0.001526 (13)	0.001856 (12)
Φ_{KJ} (Hz)	−0.009199 (21)	−0.006935 (71)	−0.011310 (68)	−0.009245 (47)	−0.007140 (72)	−0.010996 (72)
Φ_K (Hz)	0.007488 (69)	Φ_{K+} (MHz)[b] = 0.00827 (40)		[0.00708][c]	[0.00708][c]	[0.00708][c]
ϕ_j (Hz)	0.000001213 (58)	0.00000114 (11)	0.00000130 (14)	[0.00000116][c]	[0.00000116][c]	[0.00000116][c]
ϕ_{JK} (Hz)	0.0009081 (26)	0.0009708 (87)	0.0008395 (84)	0.0007997 (71)	0.0007921 (97)	0.0008050 (97)
ϕ_K (Hz)	0.009045 (65)	0.00882 (17)	0.00966 (17)	0.00850 (22)	0.00841 (28)	0.00944 (28)
L_{JJK} (μHz)	−0.00242 (10)	[−0.00242][c]	[−0.00242][c]	−0.00324 (12)	[−0.00324][c]	[−0.00324][c]
L_{JK} (μHz)	0.01754 (61)	[0.01754][c]	[0.01754][c]	0.01391 (93)	[0.01391][c]	[0.01391][c]
L_{KKJ} (μHz)	−0.1407 (34)	[−0.1407][c]	[−0.1407][c]	−0.0991(86)	[−0.0991][c]	[−0.0991][c]
ΔE (MHz)	472247.15 (11)			563787.52 (32)		
ΔE (cm^{-1})	15.7524693 (37)			18.806554 (11)		
G_a (MHz)	9708.1023 (44)			10136.164 (24)		
G_a^J (MHz)	−0.0050152 (79)			−0.004687 (16)		
F_{bc} (MHz)	−0.40297 (19)			−0.41065 (31)		
F_{bc}^K (kHz)	−0.01113 (24)			−0.00784 (38)		
G_b (MHz)	−56.8014 (77)					
G_b^J (kHz)	0.05652 (67)					
G_b^K (kHz)	−0.154 (18)					
Δ_i (uÅ^2)	0.086225 (10)	−0.182232 (19)	0.403048 (21)	0.080565 (14)	−0.191133 (37)	0.390583 (36)
N_{lines}	6701	3622	3512	4203	2919	2815
σ_{fit} (MHz)	0.043	0.050	0.049	0.034	0.046	0.046

[a] Experimental value from Ref. [7].
[b] A_-, Δ_{K-}, Φ_{K-} are arbitrarily fixed to zero as they were unable to be determined in this work.
[c] Value fixed to the ground-state value of the respective molecule.

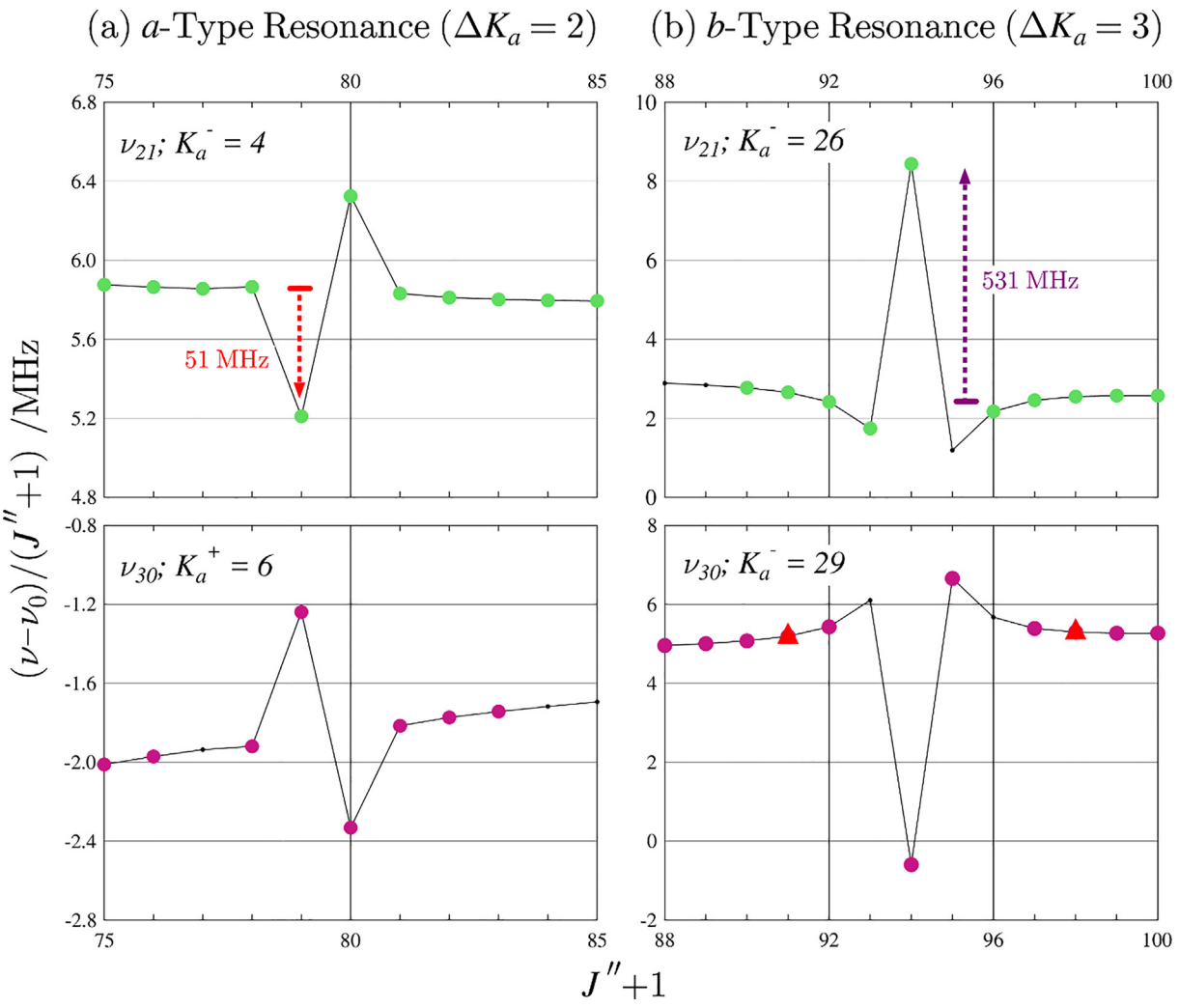

Fig. 7. Resonance plots for 3-cyanopyridine depicting measured transitions for the: (a) *a*-type resonance ($\Delta K_a = 2$) between ν_{30}, $K_a = 6^+$ (pink circles) and ν_{21}, $K_a = 4^-$ (green circles) and (b) *b*-type resonance ($\Delta K_a = 3$) between ν_{30}, $K_a = 29^-$ (pink circles) and ν_{21}, $K_a = 26^-$ (green circles). The depicted resonances are mirror images of each other at the same $J'' + 1$ value, which confirms their assignments. Dotted arrows represent the magnitudes of the resonances determined using a linear regression method. Red triangles represent data with $|(f_{obs.} - f_{calc.})/\delta f| < 3$ while filled circles represent data with $|(f_{obs.} - f_{calc.})/\delta f| > 3$. Predicted frequencies from the final coupled fit are represented by the solid black line.

There are only two pairs of matching $\Delta K_a = 5$, *b*-type resonances for 3-cyanopyridine observed in our frequency region, and they occur in the same K_a series. A resonance plot of the observed and calculated frequencies for the transitions in the $K_a = 16^-$ series of ν_{30} and the $K_a = 11^-$ series of ν_{21}, each referenced to a polynomial fit of surrounding globally, but not locally, perturbed lines and divided by $J''+1$ can be seen in Fig. 9(a). This unusual reference was required because these small resonances occur on the rising slope of very steep undulations and are otherwise difficult to recognize. A plot of the energy difference between the J values of interest is shown in Fig. 9(b) and explains the observed shapes and sequence of the two resonances in Fig. 9(a). In Fig. 9(b), the energy difference reaches zero just above $J = 65$, giving rise to a resonance with a slightly asymmetrical displacement of two resonant transitions ($J = 65 \leftarrow 64$ and $J = 66 \leftarrow 65$), one at higher and one at lower frequency, with the most perturbed energy level at $J = 65$. The energy difference climbs, then falls back across zero near $J = 70.5$, giving rise to a resonance with a slightly asymmetrical displacement of three resonant transitions with two slight displacements in one direction of the outer transitions and a larger displacement in the other direction of the central transition at $J = 71 \leftarrow 70$ (Fig. 9(a)).

6. Discussion

As is shown in Table 1 of this work and the analogous tables in previous works [1,10,11], estimation of spectroscopic constants at the B3LYP/6-311+G(2d,p) level can be expected to reliably produce useful constants for initial predictions of spectra. Experimental values for a set of analogous molecules (3-cyanopyridine, 4-cyanopyridine [1], benzonitrile [11], and phenyl isocyanide [10], Table 3) provide an opportunity to compare these species and to evaluate the computational predictions for aryl cyanides and isocyanides. Clearly there is excellent agreement in sign and order of magnitude for all experimental quartic, sextic, and octic distortion constants for these species. Determination of the quadratic force constants is sufficient to estimate the quartic centrifugal distortion terms, which using this DFT method results in quartic distortion constants with typical absolute accuracies from 3.7 to 30.3%. In each set of molecules, the percent difference

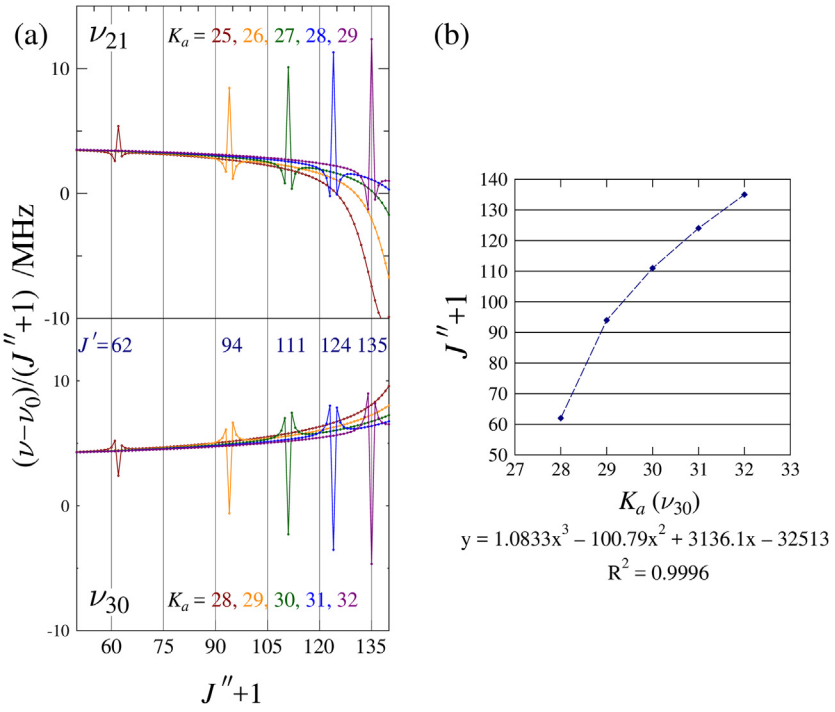

Fig. 8. (a) Superimposed resonance progressions for 3-cyanopyridine for $\Delta K_a = 3$, *b*-type resonances of the degenerate $K_a = 28–32$ series of ν_{30} (bottom) and $K_a = 25–29$ series of ν_{21} (top). (b) A plot of the most perturbed $J'' + 1$ value in each K_a series of ν_{21} versus its corresponding value of K_a.

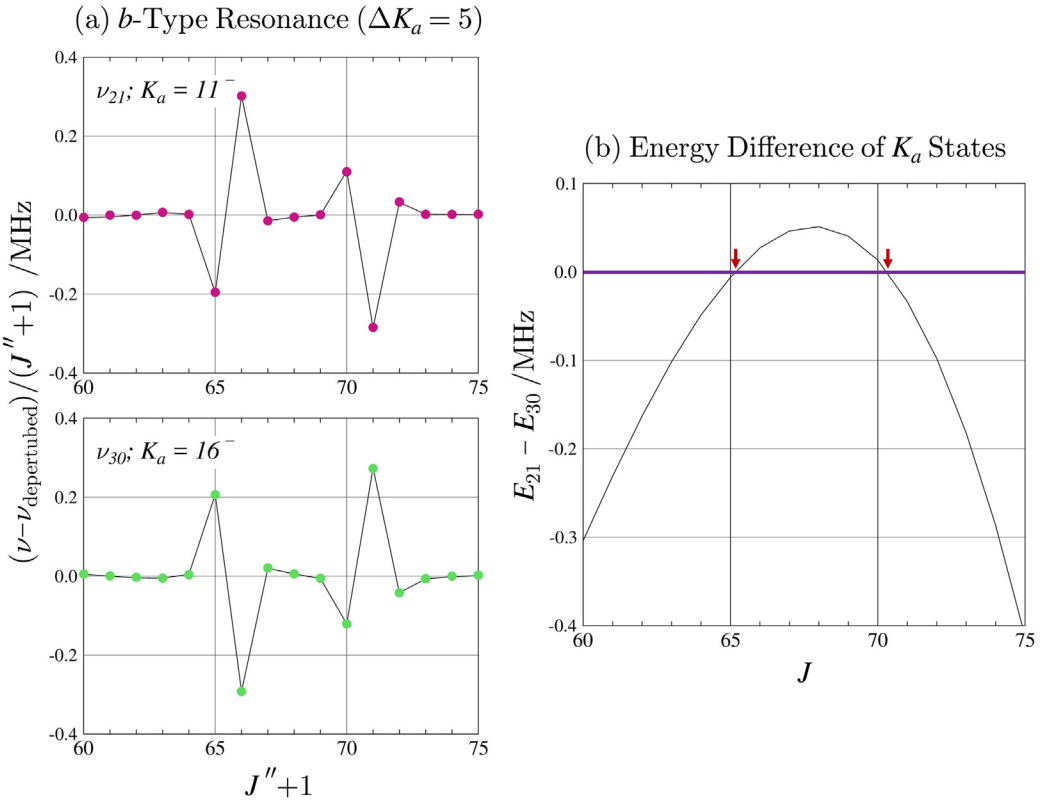

Fig. 9. (a) Resonance plots for 3-cyanopyridine depicting the experimental transitions for the $\Delta K_a = 5$, *b*-type resonance between $K_a = 16^-$ series of ν_{30} (pink circles) and the $K_a = 11^-$ series for ν_{21} (green circles). The plotted values are frequency differences between the final experimental transitions and a polynomial fit of the neighboring parts of the undulation, excluding the locally perturbed lines, all divided by $J''+1$. Specifically, the data for the polynomial fits included $J'' + 1$ from 58 to 78, excluding 64–67 and 69–72. The black lines connecting the points are the frequency differences between the final SPFIT predicted transitions and the same polynomial fit, all divided by $J'' + 1$. (b) Plot of the pertinent near-resonant K_a-series energy differences between ν_{30} and ν_{21} across $J'' + 1$ values of interest.

Table 3
Spectroscopic constants for the ground vibrational states of 3-cyanopyridine, 4-cyanopyridine, benzonitrile, and phenyl isocyanide (A-reduced Hamiltonian, I^r representation).

	3-Cyanopyridine	4-Cyanopyridine [1]	Benzonitrile [11]	Phenyl Isocyanide [10]
$A_0^{(A)}$ (MHz)	5823.05832 (11)	6000.67028 (91)	5655.265371 (75)	5659.3374 (13)
$B_0^{(A)}$ (MHz)	1571.351896 (30)	1541.180078 (12)	1546.8757804 (76)	1639.771667 (59)
$C_0^{(A)}$ (MHz)	1237.169980 (23)	1225.999666 (11)	1214.4040772 (67)	1271.154548 (49)
Δ_J (kHz)	0.0464884 (30)	0.0469997 (26	0.0452653 (27)	0.0494489 (40)
Δ_{JK} (kHz)	1.063742 (28)	0.977719 (47)	0.937906 (27)	0.912873 (36)
Δ_K (kHz)	0.23366 (16)	0.3319 (27)	0.24234 (77)	0.2605 (17)
δ_J (kHz)	0.0110955 (13)	0.01103714 (53)	0.01101589 (73)	0.0124650 (22)
δ_K (kHz)	0.673712 (34)	0.64553 (17)	0.609088 (74)	0.60134 (13)
Φ_J (Hz)	0.00000360 (12)	0.00000295 (11)	0.00000051 (22)	0.00000262 (17)
Φ_{JK} (Hz)	0.0018504 (47)	0.001718 (11)	0.0015435 (46)	0.0018134 (85)
Φ_{KJ} (Hz)	−0.009199 (21)	−0.009245 (47)	−0.007849 (17)	−0.009494 (31)
Φ_K (Hz)	0.007488 (69)	[0.00708][a]	[0.0]	[0.00755][a]
ϕ_J (Hz)	0.000001213 (58)	[0.00000116][a]	0.000001412 (38)	0.000001206 (86)
ϕ_{JK} (Hz)	0.0009081 (26)	0.0007997 (71)	0.0007431 (30)	0.0008555 (58)
ϕ_K (Hz)	0.009045 (65)	0.00850 (22)	0.007106 (76)	0.00651 (13)
L_J (μHz)	[0.0]	[0.0]	0.0000585 (56)	[0.0]
L_{JJK} (μHz)	−0.00242 (10)	−0.00324 (12)	−0.002085 (52)	−0.003943 (94)
L_{JK} (μHz)	0.01754 (61)	0.01391 (93)	[0.0]	[0.0]
L_{KKJ} (μHz)	−0.1407 (34)	−0.0991 (86)	−0.0428 (18)	−0.0327 (35)
L_K (μHz)	[0.0]	[0.0]	4.468 (90)	6.38 (15)

[a] Term fixed at the computationally predicted value.

between the experimental and DFT results [(*obs.* – *calc.*)/*obs.* × 100] is consistently negative for Δ_K, a sign that the DFT calculation regularly overpredicts the value of Δ_K to varying degrees (absolute variability 1.7–30.3%). The calculation of sextic distortion constants and the ground-state rotational constants (B_0) requires an anharmonic frequency calculation via 2nd-order vibrational perturbation theory (VPT2) to estimate the cubic and quartic force constants. As shown by this set of related works, predictions of the sextic distortion constants (typical variability 1.5–50.0%) are not as reliable as the quartic distortion constants. It is difficult to comment on the consistency in the percent difference for the sextic distortion coefficients, as not all of the related works were able to determine all sextic distortion terms in the various least-squares fits. In all previously studied C_{2v} molecules, Φ_K could not be determined and had to be held constant to the computationally predicted value. 3-Cyanopyridine is the only molecule in this group where the ground-state value of Φ_K was successfully determined experimentally, a result of the additional *b*-type, R-branch transitions present in the spectrum. It is not surprising that the purely *K*-dependent distortion parameters in the Hamiltonian, Δ_K and Φ_K, have the largest discrepancy with B3LYP predictions and are difficult to determine experimentally, as they are strongly correlated with the large *A* rotational constant. Given that these differences can be observed across several analogous species, all with low-error experimental least-squares fits, we can conclude that the deviation between the experimental and computed constants is mostly related to the DFT modeling of the geometry and force constants. A DFT model of the 3-cyanopyridine geometry can be found in the supplementary material. The observable rotational constants are well predicted with small relative discrepancies for all of the species (<0.2% for A_0, B_0, and C_0). A table of the comparison between experimental and DFT values can be found in the supplementary material.

While it is possible to use theoretical methods to predict certain spectroscopic constants (rotational constants, quartic and sextic centrifugal distortion constants), methods for predicting octic centrifugal distortion constants are not available. Estimating octic centrifugal distortion constants requires a VPT4 calculation which is not currently implemented in any available computational package. Each of the on-diagonal octic centrifugal distortion terms (L_J, L_{JJK}, L_{JK}, L_{KKJ}, and L_K) has been determined for at least one member of this series of molecules. The physical meaning of the *L* values is limited by both an incomplete determination of the sextic centrifugal distortion terms (4-cyanopyridine [1], benzonitrile [11], and phenyl isocyanide [10]) and the incomplete set of octic terms for all species. Nonetheless, these terms appear to be physically meaningful for these species due to their consistency in both sign and magnitude. As the ability of a set of constants to simply reproduce the experimental spectrum may not indicate that those constants represent the most physically meaningful solution of the Hamiltonian, it is important to carefully consider the spectroscopic constants produced by the least-squares fit. The parameter L_{JJK} in particular shows little variability across the series of molecules, from −0.00242 (10) μHz for 3-cyanopyridine to −0.003943 (94) μHz for phenyl isocyanide, lending support for its physical meaningfulness in each of the least-squares fits. The largest variability occurs for L_{KKJ} which ranges from −0.1407 (34) μHz for 3-cyanopyridine to −0.0327 (35) μHz for phenyl isocyanide. While all of these octic terms were well-determined in their respective least-squares fits, the extent of their physical meaning is uncertain. Without a larger set of experimental comparisons or an advancement in computational capabilities, it will remain unclear whether or not this variability is a natural feature of these molecules or a sign that centrifugal distortion from other sextic and octic terms not included or in these least-squares fits is being absorbed into L_{KKJ}. Comparisons and data can be found in the supplementary material

The spectroscopic constants and perturbation terms of the ground state and lowest-energy dyad for 3-cyanopyridine (ν_{30} and ν_{21}) and 4-cyanopyridine (ν_{20} and ν_{30}) are presented in Table 2. Comparing the experimentally determined quartic, sextic, and octic distortion constants of the 3- and 4-cyanopyridine isomers shows excellent agreement in sign and order of magnitude, a promising indication that all of these spectroscopic constant values are physically meaningful. Table 4 summarizes the experimental and computational perturbation terms for the analogous isolated dyads of 3-cyanopyridine, 4-cyanopyridine [1], phenyl isocyanide [10], benzonitrile [11], and two similar least-squares fits of phenyl acetylene [20]. These data show the remarkable agreement in sign and order of magnitude of all *a*-type perturbation terms across this series of molecules. The computed values all underestimate the value of G_a by 30–200 MHz, but, nonetheless, the computational estimations agree to approximately within 2% of the experimental values.

Fig. 10 displays superimposed resonance plots containing $^aR_{0,1}$ transitions in the even values of K_a from 2^+ to 30^+ of the lowest-

Table 4
Experimental and computational Coriolis-coupling constants for mono-substituted arenes.

Experimental	3-Cyanopyridine	4-Cyanopyridine [1]	Phenyl Isocyanide [10]	Benzonitrile [11]	Phenyl Acetylene[a] [20]	Phenyl Acetylene[b] [20]
G_a (MHz)	9708.1023 (44)	10136.164 (24)	9718.593 (13)	9532.0 (62)	9547.8 (32)	9710.0 (33)
G_a^J (MHz)	−0.0050152 (79)	−0.004687 (16)	−0.0058363 (44)	−0.004588 (27)	−0.0048495 (89)	−0.0047536 (79)
F_{bc} (MHz)	−0.40297 (19)	−0.41065 (31)	−0.480985 (59)	−0.411 (39)	−0.4761 (26)	−0.3518 (24)
F_{bc}^K (kHz)	−0.01113 (24)	−0.00784 (38)	−0.01520 (20)	−0.00981 (44)	−0.00394 (48)	−0.00570 (45)
G_a^K (MHz)			−0.0021119 (97)			
G_a^{JJ} (Hz)			0.00858 (12)			
G_a^{JK} (Hz)			−0.0760 (27)			
G_b (MHz)	−56.8014 (77)					
G_b^J (kHz)	0.05652 (67)					
G_b^K (kHz)	−0.154 (18)					
Computed [c]						
G_a (MHz)	9574	9943	9688	9361	9495	9495
obs. – calc.	134	193	31	171	53	214
% diff	1.4	1.9	0.3	1.8	0.6	2.2
G_b (MHz)	−56.68					
obs. – calc.	−0.12					
% diff	0.2					

[a] Solution I in Ref. [20].
[b] Solution II in Ref. [20].
[c] B3LYP/6-311+G(2d,p).

energy vibrational states of 3-cyanopyridine (ν_{30}) and 4-cyanopyridine (ν_{20}). Unlike Fig. 8, the reference states in Fig. 10 are deperturbed predictions (the same final rotational and distortion constants, but with all perturbation terms removed). In Fig. 10(a) and (b), the progression of *a*-type resonances along the bottom of the undulation can be compared for 3- and 4-cyanopyridine. The largest local perturbation in 3-cyanopyridine has a magnitude 28 × the size of the largest resonance in 4-cyanopyridine. Two of the ΔK_a = 3, *b*-type resonances shown explicitly in Fig. 8 can be seen in Fig. 10(a), in the flat region preceding the undulations in $K_a = 28^+$ (blue) and 30^+ (fuchsia). The other resonances observed in Fig. 10(a) are *a*-type resonances with even-value ΔK_a selection rules. In our recent analysis of 4-cyanopyridine, we discovered that setting the higher-order perturbation terms (G_a^J, F_{bc}^K) to zero made minimal qualitative changes in the appearance of the resonance progression [1]. While excluding the higher-order perturbation terms ($G_a^J, F_{bc}^K, G_b^J, G_b^K$) for the 3-cyanopyridine fit produces a significant quantitative effect on the perturbed frequencies and would result in a non-converging fit, that exclusion has minimal qualitative effects on the appearance of the resonance progression. On the other hand, setting both F_{bc} and F_{bc}^K to zero causes dramatic quantitative and qualitative changes to the perturbed frequencies. The *a*-type resonances grow significantly in magnitude, as demonstrated in Fig. 10(c) and (d). The same behavior was previously observed for 4-cyanopyridine and benzonitrile. As expected, setting F_{bc} and F_{bc}^K to zero made no qualitative change to the *b*-type resonances. Setting all *b*-type perturbation terms (G_b, G_b^J, G_b^K) to zero results in pronounced changes to the resonance progression [Fig. 10(e)]. All *b*-type resonances are, of course, lost. A more interesting and somewhat more subtle change is observed in the magnitude of the *a*-type resonances. There is a clear decrease in the size of the *a*-type resonances which demonstrates that the inclusion of *b*-type perturbation terms alters the predicted magnitude of *all* resonances observed in the spectrum. For 3-cyanopyridine, this effect presumably arises due to quantum mechanical interference terms between the two types of Coriolis interaction.

The contour plots demonstrate the substantial magnitude of the mixing of the states involved in 3-cyanopyridine [Fig. 11(a)) compared to 4-cyanopyridine (Fig. 11(b)]. The mapped values in Fig. 11 correspond to $(1 - P_{mix})$, where P_{mix} is the mixing coefficient of a vibration–rotation energy level. Most observable resonances occur where their state mixing is strong, manifest as islands in the contour plot with matching J'' values in each vibrational state and a difference of 2 or 4 (*a*-type) or 3 or 5 (*b*-type) in K_a. Both vibrational states of 3-cyanopyridine show prominent islands as an effect of the *a*- and *b*-type state mixing; however, the strongly perturbed *b*-type resonances are only clearly visible for $K_a'' > 24$. Along the diagonal, the regularly progressing, prominent *a*-type resonances reveal islands similar to those seen in 4-cyanopyridine (Fig. 11 (b)) and other previously studied C_{2v} species. While most resonances in 4-cyanopyridine occur at J'' >100 and are localized to the high-frequency region of the spectrum (235–360 GHz), 3-cyanopyridine displays larger resonances that appear throughout the entire frequency domain. These data further demonstrate that there is much stronger state mixing in 3-cyanopyridine compared to 4-cyanopyridine. (The mixing coefficients in 4-cyanopyridine depicted in Fig. 11(b) were manually scaled by a factor of 1.5 to enhance the appearance of the islands.) The most intriguing aspect of the contour plot for 3-cyanopyridine is the lack of symmetry between the magnitudes of the mixing coefficients in mutually perturbing islands of ν_{30} and ν_{21}. For the molecules that we studied previously, which exhibit only *a*-type Coriolis perturbations, the contour plots display a much higher degree of symmetry, *e.g.*, Fig. 11(b).

Even though 3-cyanopyridine has *a*-type resonances of much larger magnitude than 4-cyanopyridine, most nominal interstate transitions in 3-cyanopyridine associated with *a*-type resonances are still predicted to be extremely weak. The predicted intensities of these interstate transitions are half the intensity of the weakest observed transitions in the spectrum. No nominal interstate transitions associated with *a*-type resonances were strong enough to be assigned. On the other hand, two matched pairs of nominal interstate transitions associated with *b*-type resonances were assigned. A matched pair consists of nominal interstate transitions whose lower and upper rotational levels correspond to the lower and upper rotational levels of two standard, within-state $^aR_{0,1}$ transitions. To be included in the final least-squares fit, the measured nominal interstate transitions (1) had to have similar intensities in the rotational spectrum, (2) all four transitions – the pair of nominal interstate transitions and the two corresponding within-state transitions – had to be successfully incorporated into the overall data set, and (3) the average of the frequencies of the nominal interstate matched pair had to be equal within their combined measurement errors (~0.07 MHz) to the average of the correspond-

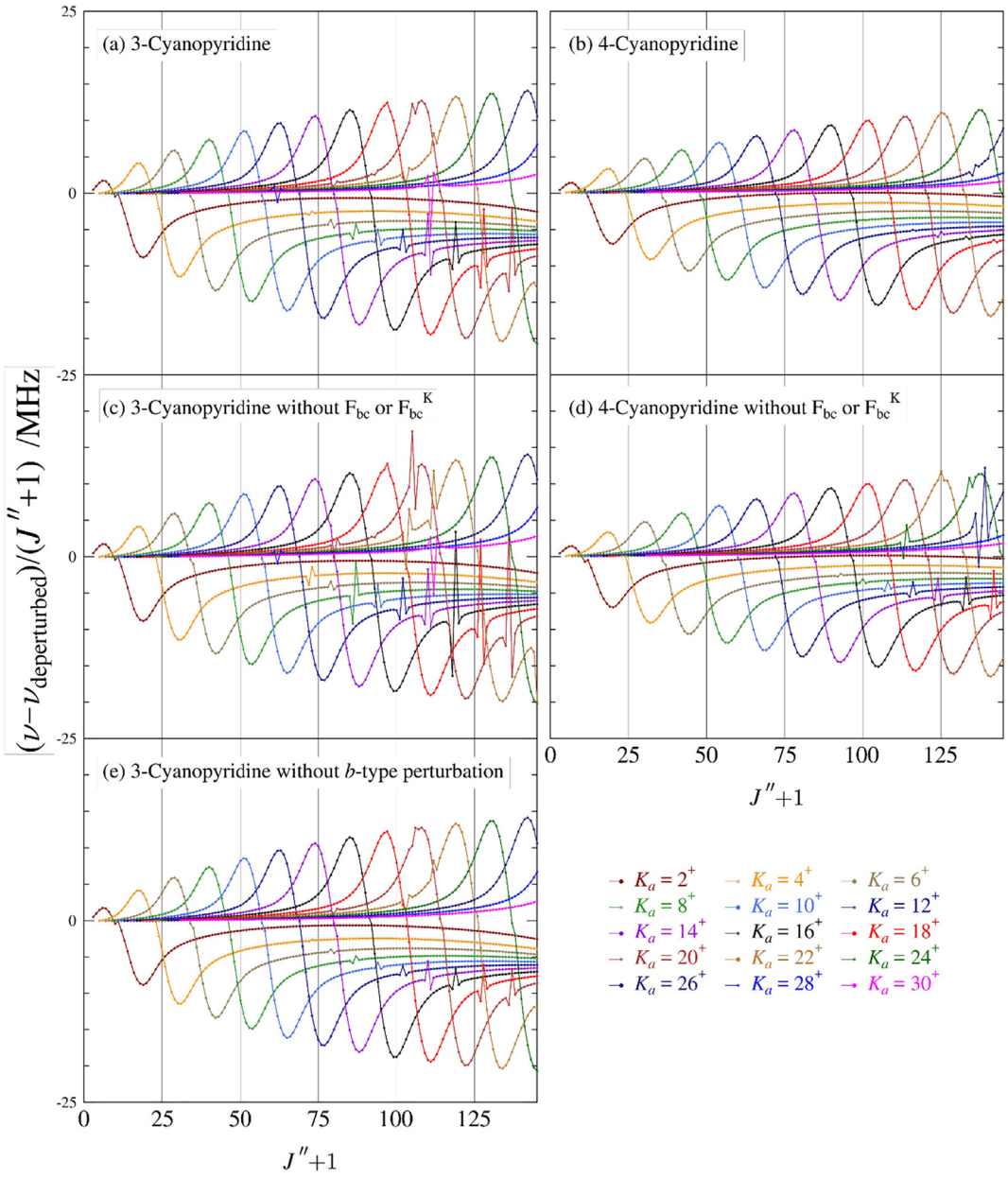

Fig. 10. Superimposed resonance plots of even K_a^+ series for the lower-energy vibrational state ν_{30} of 3-cyanopyridine (a) and ν_{20} of 4-cyanopyridine (b). For clarity, K_a series from 2^+ to 30^+ are shown with measured transitions omitted. The plotted values are frequency differences between excited-state transitions and their deperturbed counterparts, scaled by (J'' + 1).

ing within-state frequencies. The strong intensities of the formally forbidden *b*-type interstate transitions confirm that there is strong *b*-type mixing occurring between these particular K_a rotational levels in ν_{21} and ν_{30}. Compared to the predicted *a*-type nominal interstate transitions, the already large *b*-type nominal interstate intensities are further doubled by fact that they are all degenerate pairs. All nominal interstate transitions included in the least-squares fit are provided in the supplementary material, and a representative matched pair of the measured *b*-type nominal interstate transitions is illustrated in Fig. 12.

The experimentally determined vibration–rotation interaction constants, Coriolis coupling constants ($\zeta^a_{30,21}$ and $\zeta^b_{30,21}$), and energy difference between ν_{30} and ν_{21} are shown in Table 5 compared with their computational values. Properly including the *a*- and *b*-type Coriolis coupling terms in the least-squares fit of the dyad should result in rotational and distortion constants largely free of coupling effects. Due to unaddressed Coriolis coupling present in the computational value, however, the predicted *a*-axis vibration–rotation interaction constants have large opposite signs and differ substantially from the experimental values. Although the *a*-axis vibration–rotation interaction constants are not explicitly comparable, there is excellent agreement (−0.03 MHz) between the computed and experimental A_+ values, providing further evidence of untreated coupling in the computed $A_0 - A_{30}$ and $A_0 - A_{21}$ values. The computed $B_0 - B_v$ and $C_0 - C_v$ values are within 0.16 MHz of the experimentally determined values. The predicted and experimental $\zeta^a_{30,21}$ values (*obs.* − *calc.* = 0.01) and $\zeta^b_{30,21}$ values (*obs.* − *calc.* = 0.0001) display exceptional agreement. Lastly, the experimental energy difference in this work ($\Delta E_{30,21}$ = 15.7524693 (37) cm^{-1}) and the value reported from

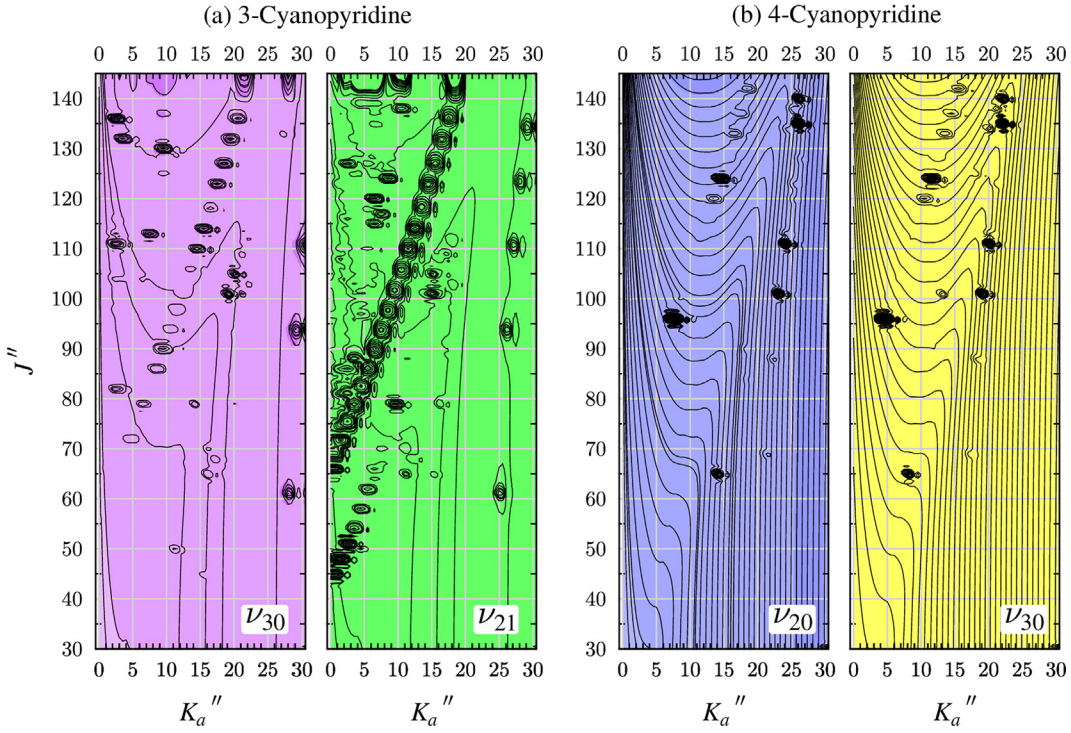

Fig. 11. Contour plots depicting the coupling landscape between rotational levels: (a) in ν_{30} and ν_{21} vibrational states of 3-cyanopyridine (violet and green, respectively) and (b) in ν_{20} and ν_{30} vibrational states of 4-cyanopyridine (blue and yellow, respectively). The mapped values are $(1 - P_{mix})$ where P_{mix} is the mixing coefficient of a given vibration–rotation energy level. The magnitude of mixing between levels in the two vibrational states are apparent as matching, similarly shaped islands along the horizontal direction (same J) but differing in the values of K_a. The mixing coefficients in 4-cyanopyridine have been scaled by a factor of 1.5 for clarity and to enhance more resonance features.

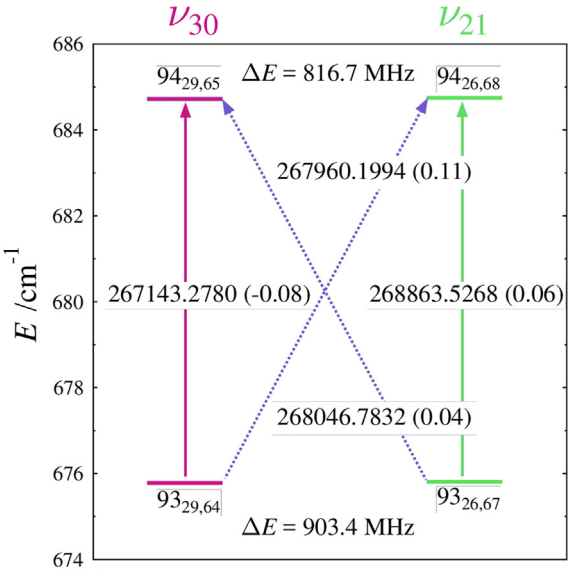

Fig. 12. Energy diagram of a matched pair of *b*-type nominal rotation-vibration transitions between ν_{30} (pink) and ν_{21} (green) vibrational states of 3-cyanopyridine. In-state $^aR_{0,1}$ vibrational transitions are denoted by vertical arrows while corresponding nominal interstate transitions are indicated by diagonal, dashed arrows. The value along each arrow corresponds to the transition frequency with the *obs. – calc.* value in parenthesis. The energy separation between the two pairs of strongly interacting rotational energy levels is given for both the lower levels (ΔE = 903.4 MHz) and the upper levels (ΔE = 816.7 MHz).

the Raman analysis (16 cm^{-1}) [6,7] match quite closely, while the predicted value is larger by ~6 cm^{-1}. The computational overestimation of the energy gap was also noted for 4-cyanopyridine [1], phenyl isocyanide [10], and benzonitrile [11].

Table 5
Experimental and computed vibration–rotation interaction constants, Coriolis-coupling constants, and energy difference for excited vibrational states ν_{30} and ν_{21} of 3-cyanopyridine.

	Experimental	B3LYP/6-311+(2d,p)	*obs. – calc.*
$(A_{30} + A_{21})/2$ (MHz)[a]	0.69114 (28)	0.72	−0.03
$A_0 - A_{30}$ (MHz)		154.53694	
$B_0 - B_{30}$ (MHz)	−1.774293 (58)	−1.73	−0.04
$C_0 - C_{30}$ (MHz)	−1.883328 (52)	−1.86	−0.03
$A_0 - A_{21}$ (MHz)		−153.09749	
$B_0 - B_{21}$ (MHz)	−3.058062 (66)	−2.90	−0.16
$C_0 - C_{21}$ (MHz)	−0.901894 (56)	−0.84	−0.06
$\zeta^a_{30,21}$	0.8327 (9)	0.82	0.01
$\zeta^b_{30,21}$	−0.0181 (3)	−0.018	0.0001
ΔE (cm^{-1})	15.7524693 (37)	21.9	6.2

[a] $(A_{30} - A_{21})/2$ is arbitrarily fixed to zero as it was unable to be determined in this work.

7. Conclusion

The very large number and types of rotational transitions measured for the ground vibrational state of 3-cyanopyridine, in combination with an analysis of centrifugal distortion (complete quartic/sextic, partial octic), now make it possible to predict the rotational spectrum of 3-cyanopyridine across its entire observable frequency range to an accuracy adequate for radioastronomical searching and identification. The reliability of these predications is expected to extend to substantially higher frequency, including transitions deep into the sub-millimeter or THz region. The exception to this broad predictably is the absence of an analysis of the quadrupole hyperfine structure due to the two ^{14}N nuclei, which would be required to predict the low frequency, low J spectrum accurately enough for optimal radioastronomical searches.

The current analysis of the Coriolis perturbations in 3-cyanopyridine (C_s) allows for interesting insights to be obtained and comparisons to be made with respect to recent treatments of more symmetrical (C_{2v}) analogs. The reduced symmetry, here, results in the presence of both *b*-type electric dipole selection rules and *b*-type Coriolis perturbations that have a substantial impact on the spectrum. Local resonances, corresponding to both $\Delta K_a = 3$ and $\Delta K_a = 5$, were observed and incorporated into the regression analysis, as were some examples of *b*-type Coriolis-allowed interstate transitions, permitting several *b*-type Coriolis parameters to be well determined and the accuracy of the energy separation (ΔE) value to be further improved. Even in the *a*-type Coriolis-allowed local resonances, the frequency displacements were substantially increased by the presence of the *b*-type Coriolis interactions. (This behavior is in stark contrast to the effect of including F_{bc} terms in the Hamiltonian, which substantially decreases the amplitude of the observed local frequency shifts, relative to ones calculated from G_a alone–both here and in the previously studied molecules.) The enhancement of the *a*-type local shifts by the *b*-type interaction terms seems clearly due to quantum interference effects. Another impact of the combined effect of two different kinds of Coriolis perturbation is the spoiling of the strong symmetry of appearance between the contour plots of mixing coefficients of the two neighboring vibrational states. In spite of the many interactions present here, ultimately the *a*-type interaction and centrifugal distortion constants determined for 3-cyanopyridine have proven remarkably consistent to those of the comparison molecules.

CRediT authorship contribution statement

P. Matisha Dorman: Formal analysis, Investigation, Writing - original draft. **Brian J. Esselman:** Formal analysis, Writing - original draft. **R. Claude Woods:** Conceptualization, Supervision, Writing - review & editing. **Robert J. McMahon:** Conceptualization, Supervision, Writing - review & editing, Funding acquisition.

Declaration of Competing Interest

The authors declare that they have no known competing financial interests or personal relationships that could have appeared to influence the work reported in this paper.

Acknowledgments

We gratefully acknowledge the National Science Foundation for support of this project (CHE-1664912) and for support of shared departmental computing resources (CHE-0840494). P.M.D thanks the University of Wisconsin-Madison Graduate School for support as an Advanced Opportunity Fellow. We thank Michael McCarthy for the loan of an amplification-multiplication chain to expand the frequency range of this work.

Appendix A. Supplementary material

Supplementary data to this article can be found online at https://doi.org/10.1016/j.jms.2020.111373.

References

[1] P.M. Dorman, B.J. Esselman, J.E. Park, R.C. Woods, R.J. McMahon, Millimeter-Wave Spectrum of 4-Cyanopyridine in its Ground State and Lowest-Energy Vibrationally Excited Dyad, ν_{20} and ν_{30}, J. Mol. Spectrosc. 369 (2020) 111274.
[2] R.G. Ford, The microwave spectra and dipole moments of the cyanopyridines, J. Mol. Spectrosc. 58 (1975) 178–184.
[3] H.S.P. Müller, F. Schlöder, J. Stutzki, G. Winnewisser, The Cologne Database for Molecular Spectroscopy, CDMS: a Useful Tool for Astronomers and Spectroscopists, J. Mol. Struct. 742 (2005) 215–227.
[4] R.T. Desai, A.J. Coates, A. Wellbrock, V. Vuitton, F.J. Crary, D. González-Caniulef, O. Shebanits, G.H. Jones, G.R. Lewis, J.H. Waite, M. Cordiner, S.A. Taylor, D.O. Kataria, J.E. Wahlund, N.J.T. Edberg, E.C. Sittler, Carbon Chain Anions and the Growth of Complex Organic Molecules in Titan's Ionosphere, Astrophys. J. 844 (2017) L18.
[5] B.A. McGuire, A.M. Burkhardt, S.V. Kalenskii, C.N. Shingledecker, A.J. Remijan, E. Herbst, M.C. McCarthy, Detection of the Aromatic Molecule Benzonitrile (*c*-C_6H_5CN) in the Interstellar Medium, Science 359 (2018) 202–205.
[6] J.H.S. Green, D.J. Harrison, Vibrational spectra of cyano–, formyl- and halogeno-pyridines, Spectrochim. Acta A 33 (1977) 75–79.
[7] M. Isaq, S. Arala, R.S. Kajal, Thermodynamics of 2- and 3-cyanopyridine from vibrational spectra, Indian J. Phys. 78B (2004) 115–119.
[8] L.S. Khaikin, N. Vogt, A.N. Rykov, O.E. Grikina, J. Demaison, J. Vogt, I.V. Kochikov, Y.D. Shishova, E.S. Ageeva, I.F. Shishkov, The Equilibrium Molecular Structure of 4-Cyanopyridine According to a Combined Analysis of Gas-Phase Electron Diffraction and Microwave Data and Coupled-Cluster Computations, Russ. J. Phys. Chem. A 92 (2018) 1970–1974.
[9] L.S. Khaikin, N. Vogt, A.N. Rykov, O.E. Grikina, J. Vogt, I.V. Kochikov, E.S. Ageeva, I.F. Shishkov, The equilibrium molecular structure of 3-cyanopyridine according to gas-phase electron diffraction and microwave data and the results of quantum-chemical calculations, Mendeleev Commun. 28 (2018) 236–238.
[10] M.A. Zdanovskaia, B.J. Esselman, R.C. Woods, R.J. McMahon, The 130–370 GHz rotational spectrum of phenyl isocyanide (C_6H_5NC), J. Chem. Phys. 151 (2019) 024301.
[11] M.A. Zdanovskaia, B.J. Esselman, H.S. Lau, D.M. Bates, R.C. Woods, R.J. McMahon, Z. Kisiel, The 103–360 GHz Rotational Spectrum of Benzonitrile, the First Interstellar Benzene Derivative Detected by Radioastronomy, J. Mol. Spectrosc. 351 (2018) 39–48.
[12] B.K. Amberger, B.J. Esselman, J.F. Stanton, R.C. Woods, R.J. McMahon, Precise equilibrium structure determination of hydrazoic acid (HN_3) by millimeter-wave spectroscopy, J. Chem. Phys. 143 (2015) 104310.
[13] B.J. Esselman, B.K. Amberger, J.D. Shutter, M.A. Daane, J.F. Stanton, R.C. Woods, R.J. McMahon, Rotational Spectroscopy of Pyridazine and its Isotopologs from 235–360 GHz: Equilibrium Structure and Vibrational Satellites, J. Chem. Phys. 139 (2013) 224304.
[14] Z. Kisiel, L. Pszczółkowski, B.J. Drouin, C.S. Brauer, S. Yu, J.C. Pearson, I.R. Medvedev, S. Fortman, C. Neese, Broadband rotational spectroscopy of acrylonitrile: Vibrational energies from perturbations, J. Mol. Spectrosc. 280 (2012) 134–144.
[15] Z. Kisiel, L. Pszczółkowski, I.R. Medvedev, M. Winnewisser, F.C. De Lucia, E. Herbst, Rotational Spectrum of *Trans-Trans* Diethyl Ether in the Ground and Three Excited Vibrational States, J. Mol. Spectrosc. 233 (2005) 231–243.
[16] H.M. Pickett, The fitting and prediction of vibration-rotation spectra with spin interactions, J. Mol. Spectrosc. 148 (1991) 371–377.
[17] Z. Kisiel, PROSPE-Programs for ROtational SPEctroscopy. http://info.ifpan.edu.pl/~kisiel/prospe.htm.
[18] M.J. Frisch, G.W. Trucks, H.B. Schlegel, G.E. Scuseria, M.A. Robb, J.R. Cheeseman, G. Scalmani, V. Barone, G.A. Petersson, H. Nakatsuji, X. Li, M. Caricato, A.V. Marenich, J. Bloino, B.G. Janesko, R. Gomperts, B. Mennucci, H.P. Hratchian, J.V. Ortiz, A.F. Izmaylov, J.L. Sonnenberg, D. Williams-Young, F. Ding, F. Lipparini, F. Egidi, J. Goings, B. Peng, A. Petrone, T. Henderson, D. Ranasinghe, V.G. Zakrzewski, J. Gao, N. Rega, G. Zheng, W. Liang, M. Hada, M. Ehara, K. Toyota, R. Fukuda, J. Hasegawa, M. Ishida, T. Nakajima, Y. Honda, O. Kitao, H. Nakai, T. Vreven, K. Throssell, J.A. Montgomery, Jr. , J.E. Peralta, F. Ogliaro, M.J. Bearpark, J.J. Heyd, E.N. Brothers, K.N. Kudin, V.N. Staroverov, T.A. Keith, R. Kobayashi, J. Normand, K. Raghavachari, A.P. Rendell, J.C. Burant, S.S. Iyengar, J. Tomasi, M. Cossi, J.M. Millam, M. Klene, C. Adamo, R. Cammi, J.W. Ochterski, R. L. Martin, K. Morokuma, O. Farkas, J.B. Foresman, D.J. Fox, Gaussian 16 rev C.01. Gaussian, Inc., Wallingford, CT, USA, 2016.
[19] J.R. Schmidt, W.F. Polik, WebMO Enterprise. 17.0.012e ed.; WebMO, LLC., Holland, MI, USA, 2017.
[20] Z. Kisiel, A. Kraśnicki, The millimetre-wave rotational spectrum of phenylacetylene, J. Mol. Spectrosc. 262 (2010) 82–88.
[21] P.M. Dorman, B.J. Esselman, R.C. Woods, R.J. McMahon, Millimeter-Wave Spectrum of 2-Cyanopyridine, manuscript in preparation.
[22] D. Papoušek, M.R. Aliev, Molecular Vibrational-Rotational Spectra. Elsevier Scientific Publishing Company, Prague, 1982.